Zhang *et al. Energy Mater* 2024;4:400042
DOI: 10.20517/energymater.2023.113

Energy Materials

Article

Open Access

Tailoring porous structure in non-ionic polymer membranes using multiple templates for low-cost iron-lead single-flow batteries

Jiaxuan Zhang[1], Amaia Lejarazu-Larrañaga[2], Fan Yang[3], Weilong Jiang[1], Mingruo Hu[1], Sheng Sui[1], Haolong Li[4], Fengjing Jiang[2,*]

[1]School of Mechanical Engineering, Shanghai Jiao Tong University, Shanghai 200240, China.
[2]Centre for Cooperative Research on Alternative Energies (CIC EnergiGUNE), Basque Research and Technology Alliance (BRTA), Alava Technology Park, Vitoria-Gasteiz 01510, Spain.
[3]SJTU Paris Elite Institute of Technology, Shanghai Jiao Tong University, Shanghai 200240, China.
[4]State Key Laboratory of Supramolecular Structure and Materials, College of Chemistry, Jilin University, Jilin 130012, Changchun, China.

[*]**Correspondence to:** Fengjing Jiang, Centre for Cooperative Research on Alternative Energies (CIC EnergiGUNE), Basque Research and Technology Alliance (BRTA), Alava Technology Park, Albert Einstein 48, Vitoria-Gasteiz 01510, Spain. E-mail: fjiang@cicenergigune.com

How to cite this article: Zhang J, Lejarazu-Larrañaga A, Yang F, Jiang W, Hu M, Sui S, Li H, Jiang F. Tailoring porous structure in non-ionic polymer membranes using multiple templates for low-cost iron-lead single-flow batteries. *Energy Mater* 2024;4:400042. https://dx.doi.org/10.20517/energymater.2023.113

Received: 22 Dec 2023 **First Decision:** 12 Mar 2024 **Revised:** 23 Apr 2024 **Accepted:** 25 Apr 2024 **Published:** 11 May 2024

Academic Editors: Xiongwei Wu, Guanjie He **Copy Editor:** Pei-Yun Wang **Production Editor:** Pei-Yun Wang

Abstract

Porous ion-selective membranes are promising alternatives for the expensive perfluorosulfonic acid membranes in redox flow batteries. In this work, novel non-ionic porous polyvinylidene fluoride-hexafluoro propylene membranes are designed for iron-lead single-flow batteries. The membranes are prepared using a multiple template approach, involving simultaneously using polyethylene glycol and dibutyl phthalate (DBP) as pore-forming templates. Their porous structure is finely tuned by adjusting the ratio of the two templates. As a result, dual-porous membranes bearing both macro and micropores are obtained. The H3520 membrane with modified porous structure attains a high proton conductivity of 43.5 $mS \cdot cm^{-1}$ and a relatively low ferric ion diffusion constant (8.61×10^{-8} $cm^2 \cdot min^{-1}$) and demonstrates the best balance between these performance-determining parameters (selectivity 5.04×10^5 $S \cdot min \cdot cm^{-3}$, higher than that of the N115 membrane). Besides, performance tests of the iron-lead single-flow single cells equipped with the dual-porous membranes show a high energy efficiency, exceeding 87.2% at its rated current density, and outstanding cycling stability over 200 charge-discharge cycles. Altogether, the mixed template method presents a promising strategy to prepare high-performance and low-cost non-ionic membranes for redox flow batteries.

© The Author(s) 2024. **Open Access** This article is licensed under a Creative Commons Attribution 4.0 International License (https://creativecommons.org/licenses/by/4.0/), which permits unrestricted use, sharing, adaptation, distribution and reproduction in any medium or format, for any purpose, even commercially, as long as you give appropriate credit to the original author(s) and the source, provide a link to the Creative Commons license, and indicate if changes were made.

Keywords: Energy storage, redox flow battery, porous membrane, ion selectivity, cost-effective

INTRODUCTION

The energy transition towards renewable energy sources is currently barred by the intermittent nature of main natural sources, namely wind and solar power. The integration of a high share of such intermittent renewable energies into the electrical grid can destabilize the network due to an unbalanced relation between power supply and power consumption[1]. Hereby, the transition to a clean energy system urgently requires the development of safe, efficient, and affordable batteries. In this context, Redox Flow Batteries (RFB) have emerged as promising candidates for large-scale stationary energy storage owing to their unique ability to decouple energy and power, modulable scalability, moderate cost of maintenance, and good cyclability[2]. In a RFB, the positive and negative electrolytes undergo redox reactions, transforming and storing electrical energy into chemical energy during charge, and releasing it during discharge[3]. Among other chemistries, iron-based flow batteries represent several advantages such as the abundance, low cost, and safety of iron-based materials[4-7]. Recently, Jiang *et al.* have developed an iron-lead (Fe-Pb) single-flow battery using $Pb/PbSO_4$ and Fe^{2+}/Fe^{3+} as the redox couples for the anode and cathode, respectively[8]. The results showed that, at relatively low current densities in the range of 20-40 $mA{\cdot}cm^{-2}$, the energy efficiency (EE) of the Fe-Pb battery could achieve 85%-90% with excellent cycling stability. Considering that only the catholyte needs to be circulated at the cathode, the pumping loss could be reduced by 50% as compared with the flow batteries with liquid electrolyte on both sides and therefore, a higher round-trip efficiency can be expected as compared to vanadium redox flow batteries. Moreover, the Fe-Pb battery uses abundant and very cheap salts as the active materials. The electrolyte of iron sulfate is nontoxic and fully recyclable. The $Pb/PbSO_4$ electrode material is in a solid state that can also be easily recycled. Therefore, the environmental impact of the Fe-Pb battery can be reduced to a minimum. The features mentioned above are essential for grid-scale energy storage and make the Fe-Pb single-flow battery a promising technology worthy of further development. However, since the battery would be working at a relatively low current density, the cost of the stack components, such as membranes and electrodes, should be significantly reduced to make the stacks cost-competitive.

The ion-conductive membrane plays a vital role in the battery, acting as a physical barrier between the positive and negative electrolytes, while allowing for the transport of charge-balancing ions, thus closing the electrical circuit of the battery[9]. The ability of the membrane to prevent crossover of redox materials and rapidly conduct ions directly affects the overall EE of the battery. As long as there is a trade-off between the permeability and the proton conductivity of the membranes, optimizing both properties is yet a great challenge in membrane technology[10]. Usually, these properties are provided by fixed charged functional groups in the polymers building up a dense or sub-nanometric pore-sized membrane, such as Nafion membranes. Alternatively, finely tuning the pore size in uncharged polymeric membranes can endow the membrane with an excellent balance between ion permeability and proton conductivity while broadening the range of material choices and reducing the cost compared to Nafion materials[11-13].

Poly (vinylidene fluoride-co-hexafluoropropylene) (PVDF-HFP) polymers possess outstanding chemical and mechanical stability and can be obtained at a significantly lower cost than Nafion materials[14,15]. The main drawback of PVDF-HFP is its relatively low proton conductivity, which arises from its high hydrophobicity and the lack of fixed charged functional groups. Accordingly, the arrangement of a porous structure is a simple, efficient, and cost-effective way to create non-charged ion transport channels in PVDF-HFP membranes[14,16].

Recently, the template method has been suggested for preparing porous membranes for Vanadium RFBs (VRFBs). This method consists of adding to the polymer mixture a pore-forming agent that is subsequently washed out from membrane film after casting. Polyethylene glycol (PEG)[16,17], phenolphthalein[18], hard spherical nanoparticles (SiO_2)[19], and ionic liquids[20] have been tested before to create porous structures. However, in most cases, an asymmetric porous structure combining macro, meso and micropores is preferred to achieve a fast proton transport while maintaining the selective barrier properties of the membrane. Commonly, asymmetric membranes are prepared with a thin dense or microporous layer on one side of the membrane providing a high selectivity, and a thicker macroporous layer on the other providing a high ion conductivity and mechanical stability[21]. Even though, due to the presence of the ultrathin ion-selective layer, the asymmetric membrane could be vulnerable to defects, scratches or punctures during membrane production or utilization, resulting in severe ion crossover.

An innovative approach was proposed by our group for creating a unique porous structure with multiple pore sizes, where micro, meso and macropores are combined in the membrane[16]. Following this idea, the multiple template method was further developed to improve the homogeneity of pore size distribution and reliability of ion selectivity, using modified combination of template molecules with tuned compatibility. This work presents a rationale pathway to create multiporous structures in low-cost and non-ionic polymer membranes via a facile fabrication procedure.

EXPERIMENTAL

Materials

PVDF-HFP (Kynar Flex 2801-00) was bought from Arkema Co. France. PEG (400), hydrochloric acid, sulfuric acid, and iron (II) sulfate heptahydrate were purchased from Sinopharm Chemical Reagent Co. Ltd. Dibutyl phthalate (DBP) was bought from Bide. Co. China. N, N-Dimethylformamide (DMF) was ordered from Lingfeng Co. China. Aluminum Trichloride was bought from General-reagent®. Iron (III) chloride was ordered from Adamas-beta®.

PVDF-HFP porous membrane preparation

Porous membranes with different contents of PVDF-HFP, PEG and DBP were prepared using a casting method. For that purpose, a certain amount of PVDF-HFP powder was dissolved in DMF to get 12 wt.% PVDF-HFP solution and stirred at 70 °C for 4 h to obtain a homogeneous PVDF-HFP solution. Then, various amounts of PVDF-HFP solution, PEG, and DBP were mixed for each casting solution. The prepared casting solutions were evenly cast on smooth and clean glass plates and subsequently dried in an oven at 80 °C for 6 h to remove the solvent. Afterward, the membranes were immersed in ethanol absolute to completely wash out the PEG and DBP templates. Finally, porous PVDF-HFP membranes were obtained. The abbreviations and compositions of the casting solutions are listed in Table 1.

Characterization methods

Compatibility of polymers

The compatibility between two polymers (R_a) is defined as the distance between the Hansen solubility parameters (HSP) of each polymer[22]. These parameters include the strength of dispersion (δ_D), polar (δ_P) and hydrogen bonding interactions (δ_H) between the molecules. HSP values of each polymer were collected from literature, and the Ra of each polymer couple (i.e., PVDF-HFP-PEG and PVDF-HFP-DBP) was calculated using[16,23]:

$$R_a = \sqrt{4(\delta_{D1} - \delta_{D2})^2 + (\delta_{P1} - \delta_{P2})^2 - (\delta_{H1} - \delta_{H2})^2} \quad (1)$$

Table 1. Abbreviations and compositions of the casting solutions used for preparing the porous membranes

Abbreviation	PEG content (wt.%)	DBP content (wt.%)
H5500	55	0
H0055	0	55
H2020	20	20
H2520	25	20
H3020	30	20
H3520	35	20

PEG: Polyethylene glycol; DBP: dibutyl phthalate.

In general, low R_a values (i.e., polymers with similar HSP) indicate a high miscibility between the polymers, and high values (i.e., polymers with considerably different HSP) represent a poor miscibility.

Morphology characterization

The surface and cross-section morphologies of the porous membranes were observed by using scanning electron microscopy (SEM, S-4800, Hitachi Limited). Before surface morphology analyses, all membrane samples were dried at 60 °C in an oven for 12 h, followed by gold sputtering treatment. Moreover, the H5500, H0055 and H3520 membrane samples were frozen with nitrogen and broken to get cross-section samples.

Aperture structure test

The aperture structure tests of porous membranes were conducted by applying the Brunauer-Emmett-Teller (BET) method on a specific surface area and using a porosity analyzer (Autosorb-IQ3). Before the test, membrane samples were dried and degassed.

Proton conductivity and area resistance measurements

The resistance of membranes was measured by Electrochemical Impedance Spectroscopy (EIS, SI 1260, Solartron) in the frequency range from 1 to 10^7 Hz at room temperature and using graphite bipolar plates as electrodes. The membrane sample, with an effective area of 7.07 cm^2, was sandwiched between two electrolyte containers filled with 3M H_2SO_4. The membranes were equilibrated in testing solution before the measurements. The proton conductivity was calculated by[24]:

$$\sigma = \frac{L}{A_{test\ memb}\Delta R} \tag{2}$$

$$\Delta R = R_0 - R_1 \tag{3}$$

where σ represents the proton conductivity of the sample membrane, $A_{test\ memb}$ is the tested membrane area, L denotes membrane thickness, and R_1, R_0 stand for the resistances measured with and without membranes, respectively.

Ferric ion permeability and ion selectivity measurements

The ferric ion diffusion constant of the membranes was tested in a two-compartment cell to compare their permeability. The membrane sample was sandwiched between the two chambers (A and B) [Figure 1]. Chamber A was filled with 80 mL solution containing 1 M $FeCl_3$ and 3 M HCl, while chamber B was filled with 80 mL solution containing 1 M $AlCl_3$ and 3 M HCl to balance the ionic strength of both solutions. The evolution of ferric ion concentration in chamber B was measured by an ultraviolet-visible (UV-vis)

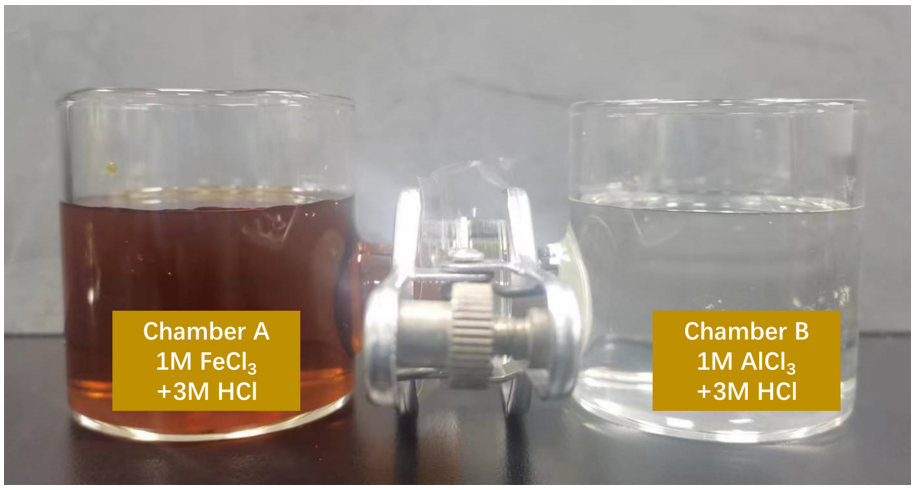

Figure 1. Fe^{3+} ion diffusion constant testing cell.

spectrometer at 420 nm. The ferric ion diffusion constant ($D_{diffusion\ const}$) was calculated using Fick's law, denoted as[24,25]:

$$V_{vol\ B}\frac{dC_B(t)}{dt} = D_{diffusion\ const}A_{test\ memb}\frac{C_A(t)-C_B(t)}{L} \quad (4)$$

where $V_{vol\ B}$ represents the volume of $AlCl_3$ solution in chamber B, $C_A(t)$, $C_B(t)$ are the ferric ion concentrations of chamber A and B at the time t, L is the thickness of the membrane, and $A_{test\ memb}$ indicates the testing area of the cell.

Ion selectivity (S_{select}) describes the ability of membranes to selectively transfer protons and to prevent the diffusion of ferric ions at the same time[23]. It was calculated by:

$$S_{select} = \frac{\sigma}{D_{diffusion\ const}} \quad (5)$$

where σ is the proton conductivity, and $D_{diffusion\ const}$ is the diffusion constant of the ferric ions through the membrane. The unit for S_{select} is Seimens·minute/cm^3 (S·min·cm^{-3}).

Tensile strength

Stress-strain curves of porous membranes were measured on a Dynamic Thermomechanical Analyzer machine (Q800, Tainstruments Co.) at 25 °C.

Iron-lead single-flow battery cell test

Charge-discharge cycling tests were carried out using a battery analyzer (Neware BTS3008W). The Fe-Pb single cell was assembled following the same procedure reported by our group[26]. Pb/$PbSO_4$ was used as a solid-state anode, and graphite felt was employed as the cathode. Both compartments were separated by the proton conductive membrane, with an effective area of 25 cm^2 [Figure 2]. The positive electrolyte consisted of 1 M $FeSO_4$ and 1.68 M H_2SO_4, and it was pumped through the cathodic chamber during charge and discharge. Nitrogen was used for degassing the electrolyte solution. The tests were performed with cut-off voltages of 0.65 and 1.1 V and at room temperature. The Fe-Pb single cell was set 30 cycles at current densities of 10, 20, 40, and 50 mA·cm^{-2}; the changes in battery efficiency at different current densities were recorded. Additionally, the long-cycle test was conducted for 200 cycles at a current density of 20 mA·cm^{-2}.

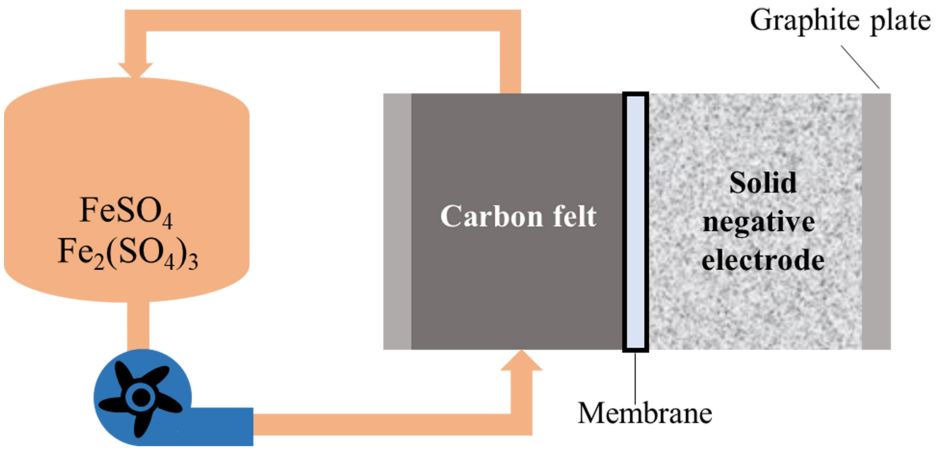

Figure 2. Schematic diagram of the Fe-Pb single-flow battery.

RESULTS AND DISCUSSION

Design of multiporous membrane with moderated proton conductivity and ion selectivity

The templating method is a widely used approach for preparing porous membranes. In the case of porous ion-selective membranes, the ion conductivity and selectivity primarily depend on the size and distribution of pores or channels within the membranes. As shown in Figure 3, larger pores or channels can enhance ion conductivity but may result in significant crossover of active molecules through the membrane. On the contrary, smaller channels may yield insufficient ion conductivity but excellent ion selectivity. Striking a perfect balance between ion conductivity and selectivity by modifying a single template poses a significant challenge.

Alternatively, this issue can be addressed by employing multiple templates, some designed to create larger pores and others responsible for smaller pores. By adjusting the ratio between these templates, ion conductivity and selectivity can be finely and continuously tuned.

The miscibility between template molecules and the polymer matrix plays a crucial role in determining the porous structure of the membrane. Often, HSP values are employed to assess the compatibility of various polymers. As shown in Table 2, the compatibility between polymers (Ra) was calculated to be 7.529 for PEG and PVDF-HFP (Ra_{HP}), whereas it was 5.784 for DBP and PVDF-HFP (Ra_{HD}). These values indicate that PEG has lower miscibility with the polymer matrix than DBP as a template[22]. Consequently, it is anticipated that using PEG as a template would result in the formation of larger pores in the membrane, enhancing ionic conductivity but potentially increasing crossover.

Conversely, employing DBP as a template would lead to the formation of smaller pores, thus improving ion selectivity at the cost of a higher membrane resistance[16,29]. Therefore, mixing both templates is expected to create a multiporous structure within the polymer membrane, combining large and small pores and thereby achieving a better balance between membrane selectivity and ionic conductivity. Table 2 shows HSP of the polymer matrix and template molecules.

Table 2. HSP values (δ_D, δ_P, and δ_H) of PVDF-HFP, PEG400, and DBP, and Ra calculation for each polymer couple

Polymer	δ_D	δ_P	δ_H	Ref.	Ra
PVDF-HFP	17.2	12.5	8.2	[27]	/
PEG400	16.6	6.3	12.3	[28]	Ra_{HP} = 7.529
DBP	17.8	8.6	4.1	[28]	Ra_{HD} = 5.784

Ra_{HP}, compatibility between PEG400 and PVDF-HFP, and Ra_{HD}, compatibility between DBP and PVDF-HFP. HSP: Hansen solubility parameters; PVDF-HFP: poly (vinylidene fluoride-co-hexafluoropropylene); PEG: polyethylene glycol; DBP: dibutyl phthalate.

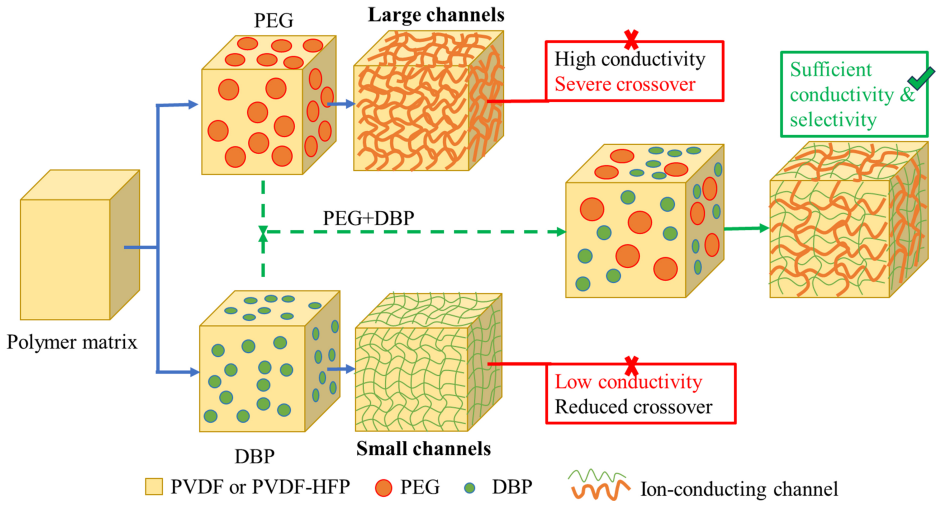

Figure 3. Illustration of the methodology employing multiple templates to achieve adjustable membrane performance in redox flow batteries. PEG: Polyethylene glycol; DBP: dibutyl phthalate; PVDF-HFP: poly (vinylidene fluoride-co-hexafluoropropylene).

Membrane morphology

The porous structure of the membranes was investigated by SEM. Figure 4 shows the top and cross-sectional views of H5500, H0055, and H3520 membranes. As predicted by the HSP, a high PEG content in the H5500 membrane [Figure 4A] resulted in the formation of large macropores. This was due to the limited miscibility between PEG and PVDF-HFP polymers. Conversely, when a high DBP content was used, as in the case of the H0055 membrane [Figure 4B], it produced a membrane with smaller and more uniformly distributed pores. This was attributed to the better compatibility between DBP and PVDF-HFP polymers[29]. Additionally, the pore distribution in the H0055 membrane was observed to be more uniform than the H5500 membrane.

As expected, combining both templates in the H3520 membrane [Figure 4C] resulted in a dual-pore structure. This structure featured a mixture of large and small pores uniformly distributed throughout the membrane, aligning with the desired outcome.

To further investigate the influence of PEG and DBP content on the porous structure of the membranes, the morphologies of the H2020, H2520, H3020, and H3520 membranes were compared in Figure 4D-G. It is evident that an increase in PEG content correlates with a higher number of macropores. Notably, the H2020 and H2520 membranes [Figure 4D and E] exhibit relatively low quantities of macropores, which can effectively isolate ferric ions but may compromise proton conductivity. Conversely, in the case of membranes prepared with higher PEG content, specifically the H3020 and H3520 membranes [Figure 4F and G], there is a significant increase in macropores. These macropores provide broader channels for rapid proton transport.

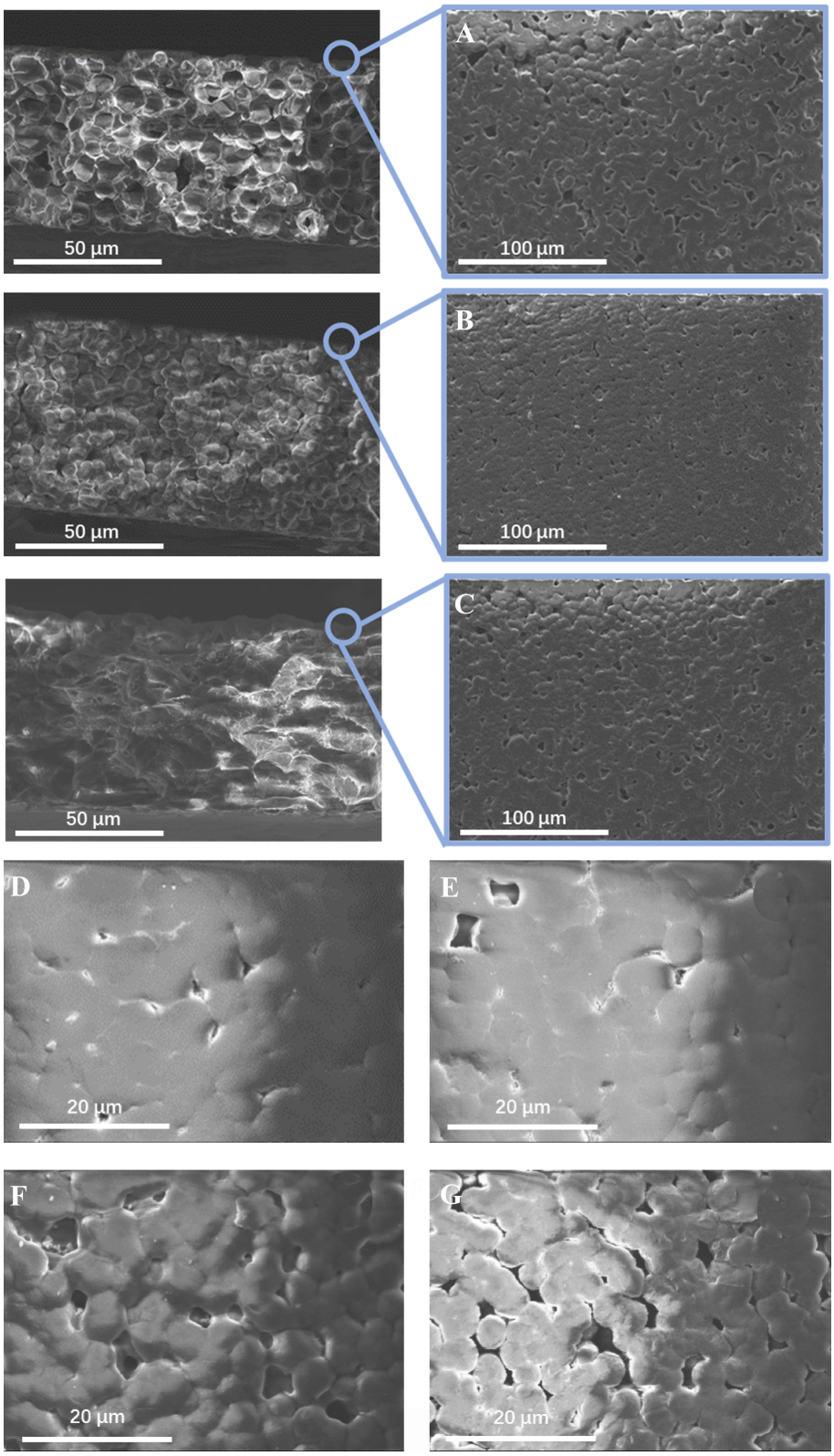

Figure 4. Cross-sectional (left) and top-view (right) SEM images of (A) porous H5500 membrane; (B) H0055 membrane; and (C) H3520 membrane. And top-view SEM images of the (D) H2020; (E) H2520; (F) H3020; and (G) H3520 membranes. SEM: Scanning electron microscopy.

Compared to membranes with a reduced macropore count (H0055, Figure 4B) and in contrast to those using PEG as the sole template (H5500, Figure 4A), the utilization of mixed templates appears to strike a better balance between ionic conductivity and selectivity.

Aperture structure test

The porous structure of membranes containing a single template (H0055 and H5500) and a mixed template (H3520) was further examined using the nitrogen adsorption-desorption method. The results for pore size distribution are presented in Figure 5. It is evident that as the PEG content increased from 0 wt.% to 55 wt.% (Figure 5A(a) and B(a), Figure 5A(b) and B(b), respectively), the peak pore diameters rapidly rose from 17.5 to 302.1 nm, confirming the direct correlation between pore size and PEG content. The H3520 membrane [Figure 5A(c) and B(c)] displays pore diameters ranging from 1.5 nm to approximately 196.3 nm, with multiple peaks in the pore size distribution, notably at 2.2 and 108 nm. These findings provide further evidence of creating a multiple porous structure resulting from using two distinct templates with varying degrees of miscibility within the polymer matrix.

Proton conductivity, ferric ion permeability, and ion selectivity

The proton conductivity, ferric ion permeability represented by diffusion constant and ion selectivity of the different membranes are displayed in Figure 6. It can be observed in Figure 6A that the proton conductivity of the porous membranes was continuously tuned by adjusting the combination use of the PEG and DBP templates. In the single template cases, H0055 with 55 wt.% DBP, and H5500 with 55 wt.% PEG, the proton conductivity of the membrane increased from around 10 $mS \cdot cm^{-1}$ to almost 60 $mS \cdot cm^{-1}$, due to the larger pores created by PEG, as illustrated above. In mixed template cases, with PEG contents from 20 wt.% to 35 wt.%, and a fixed content of DBP of 20 wt.% as a co-template, the proton conductivity of the membranes raised from 16 to 44 $mS \cdot cm^{1}$ (H2020 and H3520, respectively). As confirmed by previous results, the increase in PEG content leads to the formation of larger pores, allowing for a faster transport of ions and, thus, a higher proton conductivity of the membranes. However, the presence of wider ion transport channels necessarily reduces the ion selectivity of the membrane, leading to a higher ferric ion diffusion constant, and thus, it could compromise the capacity retention and the Coulombic efficiency of the battery. Accordingly, the H5500 membrane shows a relatively high ferric ion permeability with a diffusion constant of 1.94×10^{-7} $cm^2 \cdot min^{-1}$ compared to the commercial N115 membrane (1.53×10^{-7} $cm^2 \cdot min^{-1}$). Thanks to the moderated pore size of the membrane, the mixed template H3020 and H3520 membranes, with a dual-porous structure, demonstrated a much lower ferric ion diffusion constant of 8.37×10^{-8} and 8.61×10^{-8} $cm^2 \cdot min^{-1}$, respectively. At the same time, the proton conductivity of these membranes was kept as high as 34.8 and 43.5 $mS \cdot cm^{-1}$ for H3020 and H3520, respectively, hence reaching the best balance between conductivity and permeability properties.

The ion selectivity of the membranes was calculated according to the measured proton conductivity and ferric ion diffusion constant, and the results are displayed in Figure 6B. For the H5500 membrane (55 wt.% PEG content), the membrane selectivity fell rapidly because of the great rise in ferric ion diffusion constant. However, in the case of mixed template H3020 and H3520 membranes, an excellent balance between the ion conductivity and ferric ion permeability was reached. In fact, these membranes achieved a higher selectivity than N115 membranes (4.16×10^5 and 5.04×10^5 $S \cdot min \cdot cm^{-3}$ for H3020 and H3520 membranes, and 3.95×10^5 $S \cdot min \cdot cm^{-3}$ in the case of N115 membranes, respectively).

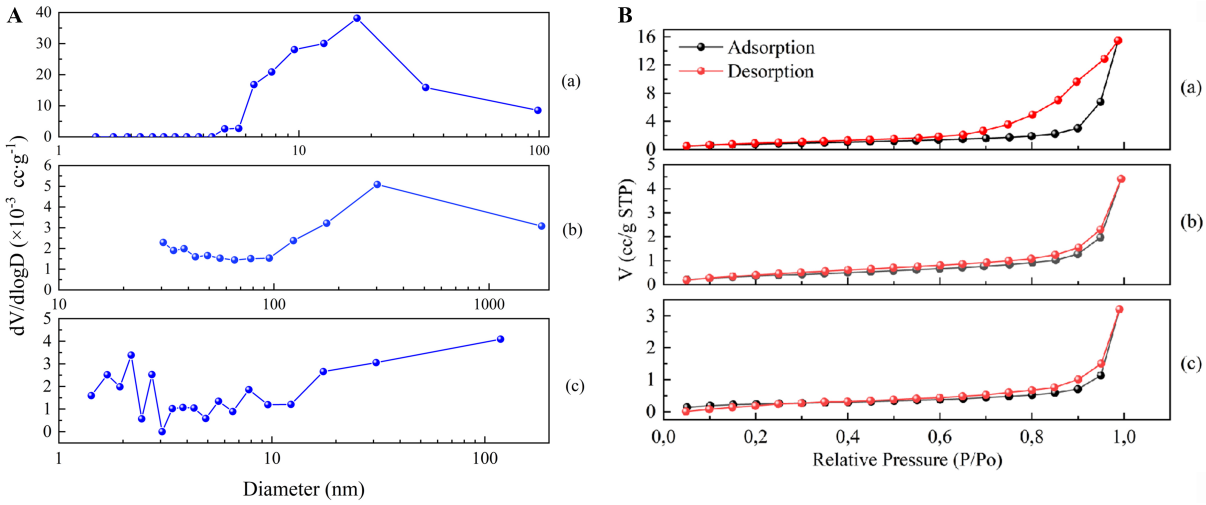

Figure 5. (A) Pore size distribution and (B) nitrogen adsorption/desorption isotherm curves of the (a) H0055; (b) H5500; and (c) H3520 membranes.

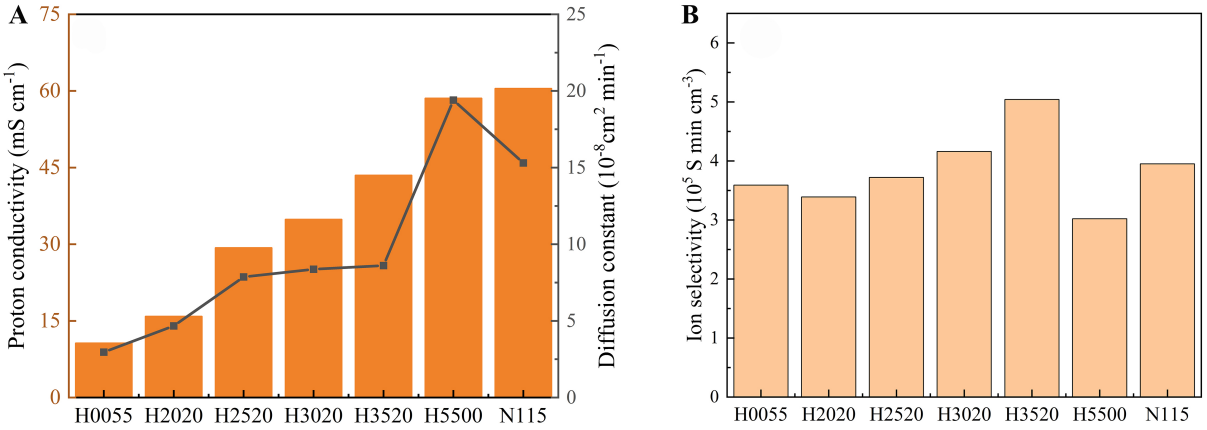

Figure 6. (A) Proton conductivity, ferric ion diffusion constant; and (B) ion selectivity of the tested membranes.

Tensile strength

The tensile strength of the membranes possessing the best selectivity (H3020 and H3520) was measured and compared with that of N115 and PVDF-HFP membranes. The tensile strength values discussed below are at a strain value of 30%. The stress-strain curves [Figure 7] showed that the as-prepared PVDF-HFP porous membranes had excellent tensile strength of 24.1 and 19.1 MPa for H3020 and H3520 membranes, respectively. The tensile strengths of these membranes were significantly higher than that of the N115 membrane (10.6 MPa). On the other hand, the variations in tensile strength indicate that the use of mixed templates influences the mechanical strength of the membranes. As compared with the tensile strength of dense PVDF-HFP membrane without pores (25.1 MPa), it can be concluded that the tensile strength of the porous membrane decreases mainly as the PEG content (associated with larger pores) increases.

Single-cell performance

With the comprehensive consideration of the analyzed membrane properties, H3020 and H3520 membranes were tested in the Fe-Pb single-flow batteries, and the battery efficiency was compared with that of the cell equipped with the N115 membrane. Figure 8 shows the coulombic efficiency (CE), voltage

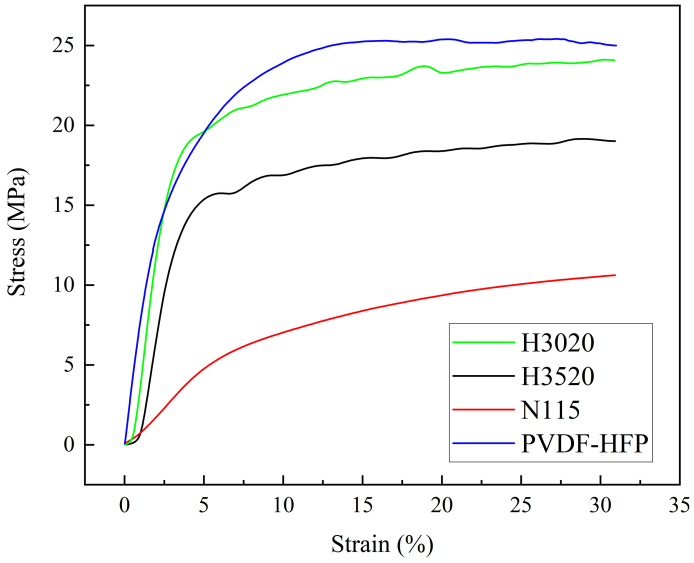

Figure 7. Stress-strain curves of the PVDF-HFP, H3020, H3520 and N115 membranes. PVDF-HFP: Poly (vinylidene fluoride-co-hexafluoropropylene).

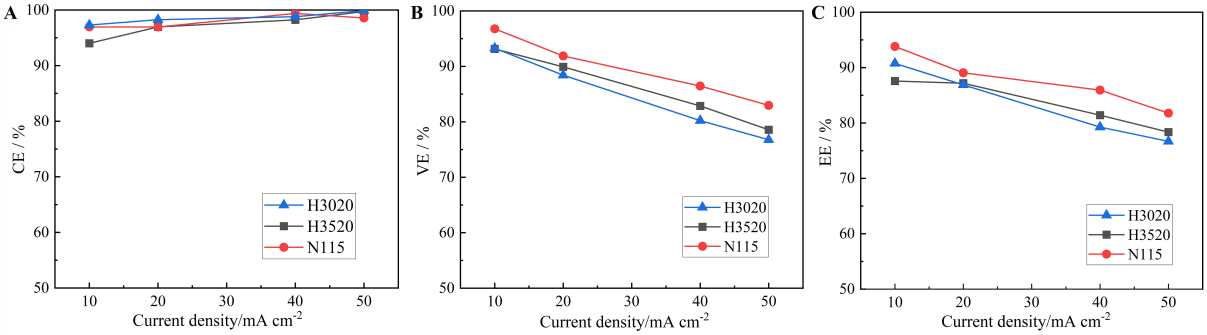

Figure 8. (A) CE, (B) VE, (C) EE of Fe-Pb single-flow batteries with H3020, 3520 porous membranes and N115 membrane, respectively, measured at various current densities. CE: Coulombic efficiency; VE: voltage efficiency; EE: energy efficiency.

efficiency (VE), and EE of the single cells at current densities ranging from 10 to 50 mA·cm^{-2}. All the cells showed excellent CE even at low current densities [Figure 8A]. Due to the higher ferric ion diffusion constant of the H3520 membrane than the H3020 membrane, CE of the former was slightly lower than that of the latter. However, as the current density increases, the difference in CE between H3520 and H3020 membranes became smaller. It is worth noting that at 50 mA·cm^{-2}, H3020 and H3520 membranes reached a CE exceeding 99.9% owing to their excellent ion selectivity. Besides, in Figure 8B, the H3520 membrane showed a higher VE than the H3020 membrane due to its higher conductivity. Furthermore, the EE of cell with the H3520 membrane shown in Figure 8C reached a comparable value of 87.2% to that of the N115 membrane measured at 20 mA·cm^{-2} (89.1% in this work and 89.22% in literature[8]).

To further study the cycling performance and stability of the porous membrane in the Fe-Pb single-flow battery, a long-term charge-discharge test over 200 cycles was conducted at 20 mA·cm^{-2}. The results presented in Figure 9 show no obvious irreversible decrease in CE, VE and EE for all the compared membranes during the 200-cycle test, indicating an excellent stability of the porous membranes in the Fe-Pb single-flow battery. It can be observed that the results of long-cycle tests are consistent with Figure 8A.

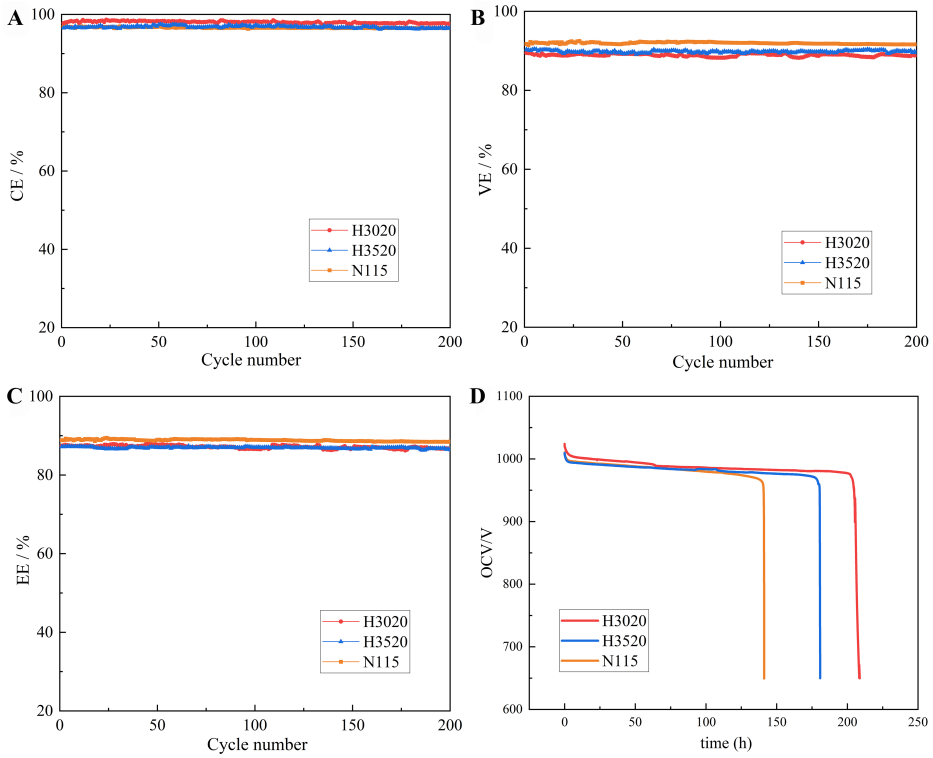

Figure 9. (A) CE, (B) VE, (C) EE of the iron-lead single-flow batteries equipped with N115, H3020 and H3520, respectively, during a 200-cycle charge-discharge test; (D) Self-discharge of the batteries with H3020, H3520 and N115 membranes. CE: Coulombic efficiency; VE: voltage efficiency; EE: energy efficiency.

Among them, the CE of N115 is around 96.1% [Figure 9A], which is lower than the 98.1% of H3020 and 96.9% of H3520. In addition, the self-discharge of the batteries with H3020, H3520, and N115 membranes was tested by measuring the time at which the open circuit voltage (OCV) decreases from 1.05 to 0.65 V; the experimental results can be observed from Figure 9D. It can be seen that the self-discharge times of H3020 and H3520 are 208.7 and 180.8 h, respectively, significantly higher than N115 membranes (141.2 h). This indicates the excellent ability of the porous membrane to prevent iron ion migration[25]. It is noteworthy that the cell with the N115 membrane exhibited bigger fluctuations in VE and EE [Figure 9B and C] than the PVDF-HFP porous membranes during the cycling measurement. This could be caused by the change of the swelling degree of the N115 membrane affected by the fluctuations of the ambient temperature. In contrast, the H3020 and H3520 membranes, composed of the non-ionic fluorinated polymer (PVDF-HFP), exhibit a minimal swelling degree due to their inherent hydrophobic nature.

Cost analysis of PVDF-HFP porous membranes and active material cost of Fe-Pb single-flow battery

Perfluorosulfonic acid (PFSA) is most widely used for redox flow batteries because of its high ionic conductivity, excellent chemical stability, and good ion selectivity. However, PFSA membranes, such as N115 (Nafion®), were reported to be around 650 \$·m^{-2}[30] in 2021, counting for a big share of the cost of the redox flow battery system[31]. Herein, the cost of PVDF-HFP porous membrane was estimated to be below 10 \$·m^{-2}, counting for 1.5% of the price of N115.

To show the economic advantages of the Fe-Pb single-flow battery, the active material cost (C) was calculated by[32]:

$$C = 3.6 \times 10^3 \frac{PM}{nFE} \quad (6)$$

Where C is the price per kilowatt-hour, P is the price per kilogram of active material, M is the molar mass of the active materials, F stands for the Faraday's constant, n represents the number of electrons, and E is the OCV of the battery. The results showed that the active material cost for the Fe-lead single-flow battery was nearly 36.35 \$·kWh^{-1}. Here, a modification was made by considering an estimated Pb usage of 50% in the anode. The active material cost of the Fe-Pb flow battery was much lower than that of VRFBs (81 \$·kWh^{-1})[30].

Considering the significantly lower cost of ion-selective membranes and active materials, the Fe-Pb single-flow battery turned out to be cost-effective and promising for large-scale energy storage.

CONCLUSION

Developing highly efficient, safe, and affordable batteries for large-scale stationary energy storage is an urgent task to enable energy transition. Ion-selective membranes are the key components of redox flow batteries. For conventional membranes, including ion-exchange and porous membranes, there is a trade-off between ion conductivity and selectivity, and it is challenging to have both high conductivity and selectivity simultaneously, especially for non-ionic porous membranes. In this work, multiporous PVDF-HFP membranes for application in Fe-Pb single-flow batteries were prepared via the mixed template method. The pore structure of the membranes was modified by adjusting the content of PEG and DBP templates. It was verified that increasing PEG content resulted in membranes with larger pores, as anticipated by HSP. As a result of mixing both templates, a porous structure featuring multiple pore sizes was obtained, where micro, meso and macropores were combined in a single layer. In such a way, the proton conductivity and ferric ion permeability of the membranes were finely tuned. H3520 mixed template membranes (35 wt.% PEG and 20 wt.% DBP) attained the best balance between these performance-determining properties and reached a high proton conductivity (43.5 mS·cm^{-1}) and a low ferric ion diffusion constant (8.61 × 10^{-8} cm^2·min^{-1}). Indeed, the ion selectivity for this was higher than that of N115, indicating a great balance of membrane properties by virtue of the arrangement of a multiple-sized porous structure. Single-cell performance tests implementing the PVDF-HFP porous membranes yield high EE (87.2% at 20 mA·cm^{-2}) and demonstrated outstanding cycling stability over 200 charge-discharge cycles. Considering the significantly lower cost and excellent chemical and mechanical stability of PVDF-HFP compared with perfluorinated sulfonic acid, the non-ionic PVDF-HFP porous membranes can notably reduce the component cost of the Fe-Pb battery, making the battery a low-cost and high-efficiency battery technology for utility-scale energy storage. Theoretically, high-performance porous membranes can be achieved by ideally manipulating the porous structure in a membrane with cost-effective polymers. As there is still room for improving the membrane performance for the Fe-Pb flow battery, future efforts should focus on further tuning the pore size and pore size distribution in the membranes to achieve higher conductivity and selectivity.

DECLARATIONS

Authors' contributions

Made substantial contributions to conception and design of the study and performed data analysis and interpretation: Zhang J, Jiang F

Performed data acquisition and provided administrative, technical, and material support: Lejarazu-Larrañaga A, Yang F, Jiang W, Hu M, Sui S, Li H

Prepared the manuscript: Zhang J, Jiang F, Lejarazu-Larrañaga A

Supervised this project: Jiang F

Availability of data and materials
Not applicable.

Financial support and sponsorship
None.

Conflicts of interest
All authors declared that there are no conflicts of interest.

Ethical approval and consent to participate
Not applicable.

Consent for publication
Not applicable.

Copyright
© The Author(s) 2024.

REFERENCES
1. Gür TM. Review of electrical energy storage technologies, materials and systems: challenges and prospects for large-scale grid storage. *Energy Environ Sci* 2018;11:2696-767. DOI
2. Sánchez-Díez E, Ventosa E, Guarnieri M, et al. Redox flow batteries: status and perspective towards sustainable stationary energy storage. *J Power Sources* 2021;481:228804. DOI
3. Guillen GR, Pan Y, Li M, Hoek EMV. Preparation and characterization of membranes formed by nonsolvent induced phase separation: a review. *Ind Eng Chem Res* 2011;50:3798-817. DOI
4. Gong K, Xu F, Grunewald JB, et al. All-soluble all-iron aqueous redox-flow battery. *ACS Energy Lett* 2016;1:89-93. DOI
5. Sinclair N, Vasil M, Kellamis C, et al. Membrane considerations for the all-iron hybrid flow battery. *J Electrochem Soc* 2023;170:050516. DOI
6. Jiang F, Zhou X, Guo D. All-iron semi-flow battery based on Fe_3O_4@CNTs 3-dimensional negative electrode. *Electrochim Acta* 2023;445:142064. DOI
7. Manohar AK, Kim KM, Plichta E, Hendrickson M, Rawlings S, Narayanan SR. A high efficiency iron-chloride redox flow battery for large-scale energy storage. *J Electrochem Soc* 2016;163:A5118. DOI
8. Jiang W, Jiang F, Zhang J, Yang F, Liu L, Hu M. Novel strategy for cathode in iron-lead single-flow battery: electrochemically modified porous graphite plate electrode. *J Energy Storage* 2024;80:110274. DOI
9. Lu W, Yuan Z, Zhao Y, Zhang H, Zhang H, Li X. Porous membranes in secondary battery technologies. *Chem Soc Rev* 2017;46:2199-236. DOI
10. Xiong P, Zhang L, Chen Y, Peng S, Yu G. A chemistry and microstructure perspective on ion-conducting membranes for redox flow batteries. *Angew Chem Int Ed Engl* 2021;60:24770-98. DOI
11. Düerkop D, Widdecke H, Schilde C, Kunz U, Schmiemann A. Polymer membranes for all-vanadium redox flow batteries: a review. *Membranes* 2021;11:214. DOI PubMed PMC
12. Zhang H, Zhang H, Zhang F, Li X, Li Y, Vankelecom I. Advanced charged membranes with highly symmetric spongy structures for vanadium flow battery application. *Energy Environ Sci* 2013;6:776-81. DOI
13. Ye J, Su J, Li H, Sun L. Chapter 5 - Recent advances in high-performance membranes for vanadium redox flow battery. In: 60 years of the loeb-sourirajan membrane. 2022. pp. 131-54. DOI
14. Ahmad AL, Farooqui UR, Hamid NA. Effect of graphene oxide (GO) on poly(vinylidene fluoride-hexafluoropropylene) (PVDF-HFP) polymer electrolyte membrane. *Polymer* 2018;142:330-6. DOI
15. Liu L, Wang F, Zhang J, et al. Boosting ion conduction in polymer blends by tailoring polymer phase separation. *J Power Sources* 2023;569:233005. DOI
16. Wang F, Zhang Z, Jiang F. Dual-porous structured membrane for ion-selection in vanadium flow battery. *J Power Sources* 2021;506:230234. DOI
17. Lin YC, Huang SL, Yeh CH, et al. Preparation of cellulose acetate/PP composite membrane for vanadium redox flow battery applications. *Rare Metals* 2011;30:22-6. DOI

18. Chen D, Li D, Li X. Hierarchical porous poly (ether sulfone) membranes with excellent capacity retention for vanadium flow battery application. *J Power Sources* 2017;353:11-8. DOI
19. Che X, Zhao H, Ren X, et al. Porous polybenzimidazole membranes with high ion selectivity for the vanadium redox flow battery. *J Membrane Sci* 2020;611:118359. DOI
20. Zhou X, Xue R, Zhong Y, Zhang Y, Jiang F. Asymmetric porous membranes with ultra-high ion selectivity for vanadium redox flow batteries. *J Membrane Sci* 2020;595:117614. DOI
21. Gubler L, Vonlanthen D, Schneider A, Oldenburg FJ. Composite membranes containing a porous separator and a polybenzimidazole thin film for vanadium redox flow batteries. *J Electrochem Soc* 2020;167:100502. DOI
22. Hansen CM. Hansen solubility parameters: a user's handbook. 2nd ed. Boca Raton: CRC Press; 2007. DOI
23. Xue R, Jiang F, Wang F, Zhou X. Towards cost-effective proton-exchange membranes for redox flow batteries: a facile and innovative method. *J Power Sources* 2020;449:227475. DOI
24. Krowne CM. Physics, electrochemistry, chemistry, and electronics of the vanadium redox flow battery by analyzing all the governing equations. *Phys Chem Chem Phys* 2024;26:2823-62. DOI
25. Krowne CM. Nernst equations and concentration chemical reaction overpotentials for VRFB operation. *J Electrochem Soc* 2023;170:100534. DOI
26. Zhang Z, Jiang F, Wu K, Shen P. Research on iron-lead semi-flow battery based on 3D solid electrode. *Acta Chimica Sinica* 2022;80:56-62. DOI
27. Bottino A, Capannelli G, Munari S, Turturro A. Solubility parameters of poly(vinylidene fluoride). *J Polym Sci B Polym Phys* 1988;26:785-94. DOI
28. Polymer handbook. 4th ed. New York: John Wiley & Sons. 1999. Available from: http://nguyen.hong.hai.free.fr/EBOOKS/SCIENCE%20AND%20ENGINEERING/MECANIQUE/MATERIAUX/COMPOSITES/Polymer_Handbook/66286_fm.pdf. [Last accessed on 9 May 2024].
29. Zeng M, Fang Z, Xu C. Effect of compatibility on the structure of the microporous membrane prepared by selective dissolution of chitosan/synthetic polymer blend membrane. *J Membrane Sci* 2004;230:175-81. DOI
30. Jiang B, Wu L, Yu L, Qiu X, Xi J. A comparative study of Nafion series membranes for vanadium redox flow batteries. *J Membrane Sci* 2016;510:18-26. DOI
31. Zhao J, Wang J, Sun L, Chen Q, Lu H. Novel low-cost cation exchange membrane containing hydrophilic cross-linked structure for enhanced electrodialysis properties. *J Taiwan Inst Chem Eng* 2019;100:269-76. DOI
32. Huskinson B, Marshak MP, Suh C, et al. A metal-free organic-inorganic aqueous flow battery. *Nature* 2014;505:195-8. DOI PubMed